Platinum surface instabilities and their impact in electrochemistry
Valls Mascaro, F.

Outlook

The work presented in this thesis addresses the (in)stability of platinum electrode surfaces at the atomic-scale with the help of EC-STM. Our findings not only contribute to improve the current understanding on the degradation of platinum catalysts, but also challenge the established assumption that stepped surfaces are composed by an array of homogeneously distributed steps. Moreover, in Chapters 3 and 4 we show how the step bunching instability has significant effects on the electrochemistry of platinum stepped surfaces, and can explain the non-linear step density-dependent trends reported in the literature. The next sections present suggestions for future studies that I collected during my PhD time, as well as measurements and insights that I performed, but could not finish within the framework of this thesis. The latter will be part of future work and publications.

O.1   Platinum Oxide Structure

In Chapter 2 we discuss that platinum surface degradation is closely related to its oxidation, which results firstly in the reversible place exchange (PE_{rev}) between platinum surface atoms and the oxygen atoms adsorbed, and ultimately in the formation of adatom and vacancy islands. Therefore, identifying the surface oxide structure is key to gain insight on the degradation mechanism, which would allow for the design of more stable catalysts.

In Chapter 4 we show that the oxidation process results in PtO_2 along the steps. However, the oxide structure on terraces remains under discussion. Surface X-Ray Diffraction (SXRD) measurements in electrochemical environment suggest that the PE_{rev} takes place randomly, similar to a 2D adatom gas, although they can not discard the formation of semi-ordered structures such as one-dimensional rows [1, 2]. These oxide rows have been observed on Pt(111) with STM at 1 bar of oxygen pressure and high temperature [3]. Moreover, their stability at high electrochemical potential is supported by DFT [4].

EC-STM measurements on Pt(111) at high oxidative potentials could be useful to capture, *operando*, the real surface oxide structure. In addition, it should be possible to follow the terrace oxidation with EC-STM while the electrode potential is increased, and then decreased, similar to the measurements performed by Wakisaka et al. [5]. A more detailed study, zooming-in on the platinum terrace, with a very sharp STM-tip, and at the optimal

tunneling conditions (e.g. high tunneling current), could provide an answer on weather the oxide rows exist, or contrary the terrace oxidation proceeds randomly.

O.2   Nucleation and Growth of Vacancy Islands

The roughening of a Pt(111) surface upon oxidation-reduction cycling was followed in detail with EC-STM [6–8]. However, while it was possible to fully characterize the adatom islands, the individual vacancies as well as small vacancy islands formed during the first cycles were most of the times not visible. The reason for this is tip convolution (i.e. any STM image results from the convolution of the tip shape and the surface morphology), which leads to the vacancies appearing smaller (both narrower and less deep) than they actually are in reality. Nevertheless, these small vacancies are known to be very active towards the ORR [9], and therefore it is important to gain insight on their nucleation, growth, and coalescence. This could be achieved using SXRD [10].

O.3   Stability of Platinum Stepped Surfaces during Oxidation-Reduction Cycling

Although there is extensive research on the roughening of Pt(111) upon oxidation-reduction cycling, there is not yet any study addressing the same cycles also on stepped platinum surfaces. However, we know that steps have a crucial role on the roughening process, as the late growth of 3D islands is dominated by the step oxidation, which results in the formation of adatoms from step atoms. In an ongoing project, we use EC-STM to study the stability of Pt(111)-vicinal surfaces upon oxidation-reduction cycling.

Figure O.1(a-e) shows 80 oxidation-reduction cycles (ORCs) on Pt(111) as well as on four Pt(111)-vicinal surfaces: Pt(15 15 14), Pt(554), Pt(553), and Pt(533), with nominal terrace widths of 30, 10, 5, and 4 atomic rows, respectively. We do know in the meantime (Chapter 3) that Pt(553) undergoes step bunching, and hence exhibits mostly terraces with double of the nominal width. Pt(15 15 14), Pt(554), and Pt(553) (as-prepared) surfaces present steps with (111) microfacets. This is evident from their initial Cyclic Voltammograms (CVs), which show a (111) step-related peak at around 0.128 V, within the Hydrogen underpotential deposition (H_{upd}) region. Contrary, the nominal structure of Pt(533) presents steps with (100) microfacets, which contribute to the (100) step-related peak at around 0.280 V. However, the first CV on Pt(533) also shows a feature at around 0.128 V, which indicates that the (100) steps on this surface are partially faceted, resulting in regions with (111) steps.

On Pt(15 15 14), oxidation-reduction cycling leads to significant changes in the electrochemical fingerprint, similarly to Pt(111). The (111) step peak in the H_{upd} region (H1 peak in Fig. O.1b) grows in intensity and becomes broader, indicating an increase of (111) step length. Moreover, three more peaks (H2-H4) appear, which were previously attributed to hydrogen desorption from single vacancies, narrow facets with (100) steps, and narrow facets with (111) steps [11]. In addition, peaks appear between 0.85 V and 1.05 V that are attributed to the oxidation of platinum step sites, as discussed in Chapter 4. Finally, the

feature related to the PE$_{rev}$ at around 1.1 V diminishes in height, indicating a decrease of terrace sites at the expense of the newly formed step sites.

On Pt(554), the CV changes much less upon oxidation-reduction cycling. The H1 peak does not increase in height, it only becomes broader. Moreover, the H2 and H3 peaks are barely visible, while the H4 peak does not appear at all. This suggests that the Pt(554) surface roughens less (or slower) than Pt(111) and Pt(15 15 14), which have wider terraces. This effect is even more notable on Pt(553), which CV barely changes during cycling. Therefore, from the ORCs one would expect that Pt(553) is stable and does not roughen at all.

Pt(533) is a special case, as it initially presents (100) steps. During oxidation-reduction cycling, (111) steps form at the expense of the (100) steps, which leads to a decrease of the H2 peak and an increase of the H1 peak [6, 12]. Apart from this, the rest of the CV barely changes during cycling, which could indicate that the terraces do not roughen.

Following the work by Jacobse et al. [6], we then quantified for all surfaces the total H$_{upd}$ charge, $Q_{H_{upd}}$, at each ORC, see Fig. O.1f. Focusing first on Pt(111), in black, the rise of $Q_{H_{upd}}$ is indicative for an increase of the surface roughness. A change on the slope of the $Q_{H_{upd}}$ curve points out towards a change of the growth speed, and thus of the roughening mechanism. Therefore, the roughening process was divided in two different regimes: the initial nucleation and early lateral (2D) growth of islands and, after around 20 cycles, the late growth that occurs predominantly in height (3D). The plateau observed in between ORCs 8-14 is related to the transition from the 2D growth into the 3D growth.

Moving now to the Pt(111)-vicinal surfaces, Pt(15 15 14) exhibits a lower slope of the $Q_{H_{upd}}$ curve than Pt(111), both in the 2D and the 3D regime, which indicates that the roughening on Pt(15 15 14) is slower. The growth speed decreases even more for Pt(554), which has a smaller terrace width, of 10 atomic rows. For Pt(553), with a nominal terrace width of 5 atomic rows (although we know from Chapter 4 that more than half of the terraces are double this value), $Q_{H_{upd}}$ increases only during the 2D regime, and not during the 3D regime. This suggests that, if islands are formed on this surface, they only grow laterally and not in height. Moreover, it shows that the narrower the terrace width, the slower the growth speed. Finally, although the ORCs of Pt(533) (with (100) steps) show remarkable changes due to the faceting of (100) steps into (111) steps, $Q_{H_{upd}}$ remains almost constant, suggesting that this surface does not roughen at all.

Figure O.2 shows EC-STM images obtained on Pt(554), Pt(553), and Pt(533) before any ORC (a-c), after 20 ORCs (d-f), and after 80 ORCs (g-i). Starting with Pt(554), the initial parallel steps on the pristine surface meander upon oxidation-reduction cycling, becoming highly rough already on cycle 20. Moreover, islands form due to the *pinching off* of the step meanders, which is driven by the attractive step-step interaction of opposite type of steps [13–15]. These islands acquire a height spanning multiple atomic layers during cycling, see Fig. O.2g. Consequently, the total step length increases, which explains the increase of $Q_{H_{upd}}$ upon cycling shown in blue in Fig. O.1f.

As elaborated in Chapter 3, more than half of the steps on the pristine Pt(553) surface, shown in Fig. O.2b, are bunched. Oxidation-reduction cycling results once again in step meandering and the subsequent breaking down of the step meanders into small islands,

as evident from Fig. O.2e. In this case, however, the roughening of this surface is less pronounced than on Pt(554) and the islands do not seem to increase in height even after 80 ORCs. This would explain that $Q_{H_{upd}}$ only rises during the 2D regime, and not in the 3D regime.

Finally, Pt(533), which should consist of (100) steps and terraces with a width of 4 atomic rows, does not present the nominal surface structure (see Fig. O.2c). Instead, this surface exhibits step meanders, which must form not only (100) but also (111) microfacets, explaining the (111) step peak in the initial CV shown in Fig. O.1e. Moreover, the terraces are visibly wider than 4 atomic rows, suggesting that the steps are bunched. Mild oxidation-reduction cycling (20 ORCs) results into the breaking down of the steps into zig-zag structures with two different orientations (Fig. O.2f). This process results in a decrease of the (100) step length and an increase of the (111) step length, which matches the observations from the ORCs in Fig. O.1e. After 80 ORCs, the initial direction of the steps is completely lost, see Fig. O.2i. Instead, the surface exhibits lines orthogonal to the initial step direction shown in Fig. O.2c. This is surprising, given the fact that the terrace atoms on Pt(533), like on any other (111)-vicinal surface, present an hexagonal arrangement with a 60 degree symmetry. Moreover, such morphological surface changes are not reflected on the $Q_{H_{upd}}$ curve shown in purple in Fig. O.1f, which remains almost constant. This suggests that the adsorption/desorption of hydrogen per total step length (i.e. sum of (100) and (111) step length) does not change during cycling, although this seems very unlikely. In order to obtain more insight, in the near future we will perform a detailed analysis on the step structure as well as on the surface roughness evolution.
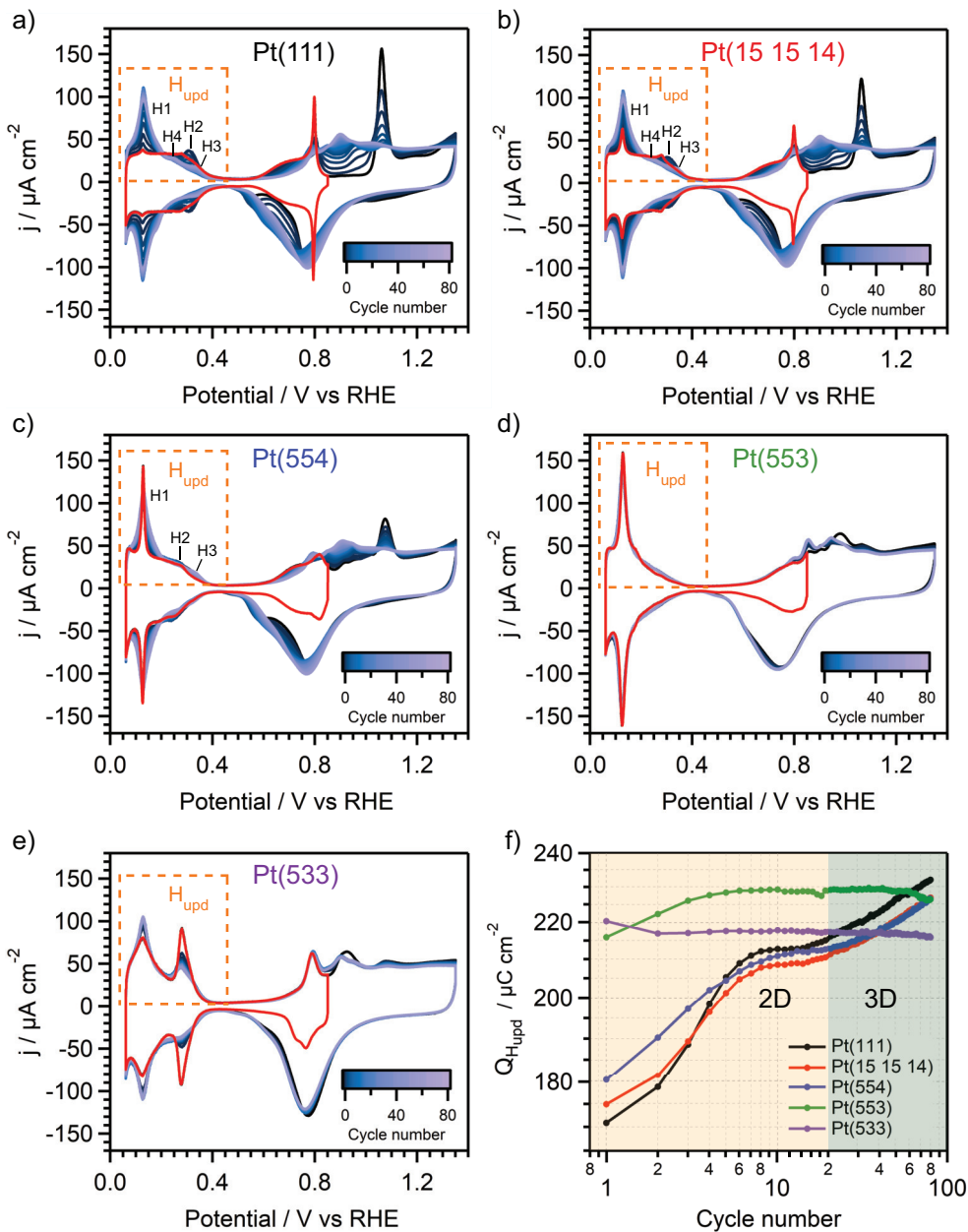
Figure O.4: Oxidation-Reduction Cycles on Pt(111) and its Vicinal Surfaces. **(a-e)** Oxidation-reduction cycles on Pt(111), Pt(15 15 14), Pt(554), Pt(553), and Pt(533). The H_{upd} region is highlighted with an orange rectangle, while the step-related peaks within are indicated as H1-H4. **(f)** The H_{upd} charge versus the cycle number (for each of the surfaces studied) is a good electrochemical measure for the roughness [6]. The two roughening regimes, in 2D and in 3D, are indicated in yellow and green, respectively.
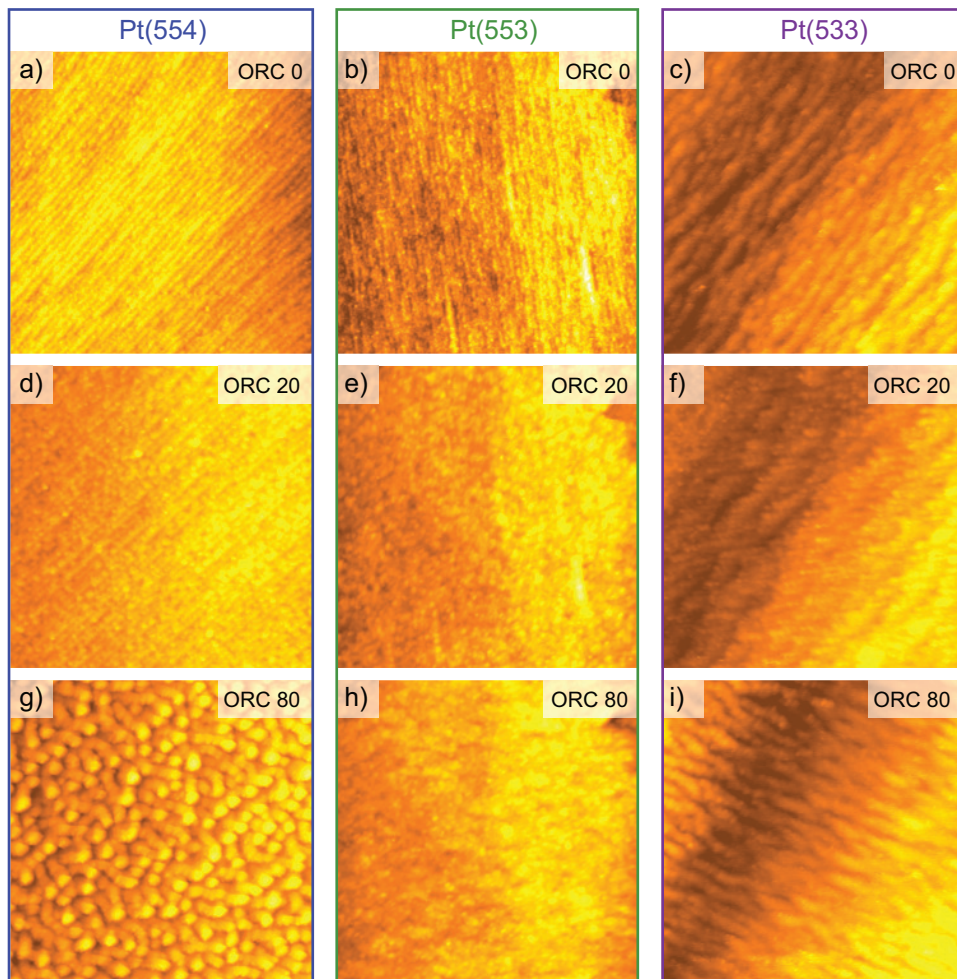
Figure O.5: EC-STM Images of Pt(111)-Vicinal Surfaces after Oxidation-Reduction Cycles. (a), **(b)**, and **(c)** show the as-prepared Pt(554), Pt(553), and Pt(533) electrodes, respectively. **(d)**, **(e)**, and **(f)** show the same samples on the same place after 20 ORCs. Finally, **(d)**, **(e)**, and **(f)** show again the same place on the surfaces after 80 ORCs. All images are 100 x 100 nm^2, and were recorded in 0.1 M HClO$_4$ at sample and tip potentials of 0.1 V and 0.15 V, respectively.

References

[1] L. Jacobse, V. Vonk, I. T. McCrum, C. Seitz, M. T. M. Koper, M. J. Rost, and A. Stierle, *Electrochim. Acta*, **407**, 139881 (2022).

[2] J. Drnec, M. Ruge, F. Reikowski, B. Rahn, F. Carlà, R. Felici, J. Stettner, O. M. Magnussen, and D. A. Harrington, *Electrochim. Acta*, **224**, 220 (2017).

[3] M. A. van Spronsen, J. W. M. Frenken, and I. M. N. Groot, *Nat. Commun.*, **8**, 429 (2017).

[4] S. Hanselman, I. T. McCrum, M. J. Rost, and M. T. M. Koper, *Phys. Chem. Chem. Phys.*, **22**, 10634 (2020).

[5] M. Wakisaka, S. Asizawa, H. Uchida, and M. Watanabe, *Phys. Chem. Chem. Phys.*, **12**, 4184 (2010).

[6] L. Jacobse, Y. F. Huang, M. T. M. Koper, and M. J. Rost, *Nat. Mater.*, **17**, 277 (2018).

[7] M. J. Rost, L. Jacobse, and M. T. M. Koper, *Nat. Commun.*, **10**, 5233 (2019).

[8] F. Valls Mascaró, I. T. McCrum, M. T. M. Koper, and M. J. Rost, *J. Electrochem. Soc.*, **169**, 112506 (2022).

[9] F. Calle-Vallejo, J. Tymoczko, V. Colic, Q. Huy Vu, M. D. Pohl, K. Morgenstern, D. Loffreda, P. Sautet, W. Schuhmann, and A. S. Bandarenka, *Science*, **350**, 185 (2015).

[10] K. Iizuka, T. Kumeda, K. Suzuki, H. Tajiri, O. Sakata, N. Hoshi, and M. Nakamura, *Commun. Chem.*, **5**, 126 (2022).

[11] L. Jacobse, M. J. Rost, and M. T. M. Koper, *ACS Cent. Sci.*, **5**, 1920 (2019).

[12] A. Björling and J. M. Feliu, *J. Electroanal. Chem.*, **662**, 17 (2011).

[13] T. Michely and J. Krug, *Islands, Mounds and Atoms*, Springer, Amsterdam (2004).

[14] M. Rost, P. Smilauer, and J. Krug, *Surf. Sci.*, **369**, 393 (1996).

[15] J. Kallunki and J. Krug, *Europhys. Lett.*, **66**, 749 (2004).